Biomicrofluidics

Lab-on-a-disk extraction of PBMC and metered plasma from whole blood: An advanced event-triggered valving strategy

Cite as: Biomicrofluidics **15**, 064102 (2021); https://doi.org/10.1063/5.0066128
Submitted: 08 August 2021 • Accepted: 10 October 2021 • Published Online: 09 November 2021

Rokon Uddin, David Kinahan, Jens Ducrée, et al.

Biomicrofluidics ARTICLE scitation.org/journal/bmf

Lab-on-a-disk extraction of PBMC and metered plasma from whole blood: An advanced event-triggered valving strategy

Cite as: Biomicrofluidics 15, 064102 (2021); doi: 10.1063/5.0066128
Submitted: 8 August 2021 · Accepted: 10 October 2021 ·
Published Online: 9 November 2021

Rokon Uddin,[1,a)] David Kinahan,[2] Jens Ducrée,[3] and Anja Boisen[1,2]

AFFILIATIONS

[1]Department of Health Technology, Technical University of Denmark, Kongens Lyngby, Denmark
[2]Department of Mechanical and Manufacturing Engineering, Dublin City University, Glasnevin, Dublin 9, Ireland
[3]FPC@DCU—Fraunhofer Project Center at Dublin City University, Glasnevin, Dublin 9, Ireland

[a)]**Author to whom correspondence should be addressed:** rokon.deen@gmail.com. **Tel.:** +358465756283

ABSTRACT

In this paper, we present a centrifugal microfluidic concept employing event-triggered valving for automated extraction of metered plasma and peripheral blood mononuclear cells (PBMCs). This "lab-on-a-disk" system has been developed for retrieving different density layers from a liquid column by "overflowing" the layers sequentially using the pressure exerted by a density-gradient liquid. Defined volumes of plasma and PBMCs were efficiently forwarded into designated microfluidic chambers as a sample preparation step prior to further downstream processing. Furthermore, the extracted PBMCs were counted directly on-disk using an automated optical unit by object-based image analysis, thus eliminating the requirement for the post-processing of the extracted PBMCs. This study is a direct continuation of our previous work[1] where we demonstrated combined on-disk detection of C-reactive protein and quantification of PBMCs following on-disk extraction of plasma and PBMCs from a single blood sample using a centrifugo-pneumatic valving mechanism. However, the former valving technique featured limited PBMC extraction efficiency. Here, integrating the novel concept along with event-triggered valving mechanism, we eliminated the occurrence of a specific microfluidic effect, which led us to increase PBMC extraction efficiency to 88%. This extraction method has the potential to be utilized for efficiently separating multiple density layers from a liquid sample in relevant biomedical applications.

I. INTRODUCTION

Within the microfluidics community, the centrifugal platform[2,3] has been of increasing impact in academia and industry over the recent decades. This interest is driven primarily by the unique advantages of the platform over conventional pressure driven microfluidic systems. Using centrifugal force for pumping, it requires just a low-cost spindle motor for operation rather than specialized pumps. In addition, the challenge of "world to chip" interfacing is mitigated as the disks can be loaded at atmospheric pressure using a simple pipet or a syrette. These advantages make the platform particularly suitable for point-of-use applications in biomedical diagnostics[4] and decentralized on-site testing of various biosamples.[5] Another particular advantage of the centrifugal platform is its inherent capability to process blood through phase separation under artificial gravity conditions induced by rotation. Plasma separation from a whole blood sample utilizing centrifugal force is one of the earliest and very common applications of centrifugal microfluidics in biomedical research.[6–8] In addition, separation of white blood cells (WBCs) from whole blood on a microfluidic disk also has been demonstrated in a few studies followed by performing cell count on-disk or out-of-disk.[9–13]

From the clinical significance perspective, the separation of WBCs or peripheral blood mononuclear cells (PBMCs) from whole blood leading to the total and differential WBC count as well as the PBMC count are markers for different clinical conditions including severe diseases like different types of inflammation/infections, coronary heart disease, cancer, immune system disorder, and HIV. However, the standard procedure in clinical laboratories to perform PBMC counting involves a number of complex and time-consuming pre-treatment steps like red blood cell (RBC) lysis,

fluorescent labeling, and staining. Thus, there is a significant need for a much simpler method to perform PBMC separation from whole blood, which does not require complex sample pre-treatment and is more automated, i.e., requiring negligible manual intervention, faster, and much cost-effective. In this regard, in our previous study,[1] we developed a novel biosensing platform that combined the plasma and PBMC extraction from single blood samples followed by automated plasma metering and utilization of the metered plasma as a sample for on-chip biomarker detection and utilization of the extracted PBMC for on-chip cell counting (CC). There, the detection of C-reactive protein (CRP) in combination with PBMC quantification from a single blood sample on a single microfluidic disk was established. Only few microliters of diluted blood was used as the initial sample, which was fractionated into plasma and PBMCs through a density-gradient media (DGM)-based centrifugation method followed by on-disk extraction of metered plasma and PBMCs into separate microfluidic chambers. On-disk CRP detection was performed by magnetic nanobead-based agglutination assay[14–23] using an integrated Blu-ray based opto-magnetic reader unit;[14,21,22,24–26] the extracted PBMCs were quantified on-disk using an integrated and automated optical imaging unit.[14,27,28] The entire biosensing platform resembled an analytical toolbox with a potential to detect different biomarkers in combination with PBMC counting from a single sample. However, the PBMC extraction efficiency was 27% lower than a standard clinical measurement due to a particular microfluidic effect. In order to extract plasma and PBMCs after blood fractionation, a centrifugo-pneumatic valving method was used where the expansion of pressurized air in a pneumatic chamber pushed the plasma and PBMCs out of the blood processing (BP) chamber through a siphon channel; and during the extraction process, a certain fraction of PBMCs remained back in the chamber and thereby decreased the extraction efficiency. Similar microfluidic phenomena were observed in Ref. 13 while using a similar valving mechanism to extract PBMCs from fractionated blood in a microfluidic disk. The phenomenon termed "phase switching effect"[13] describes that, while drawing PBMCs out of the BP chamber through the siphon, the siphon switched to drawing additional plasma instead of PBMCs; this way, some PBMCs remained in the BP chamber. However, a study[12] showed that if fractionated components of blood are not extracted/transferred from the BP chamber to another chamber, then this DGM-based centrifugation method shows high potential for WBC separation efficiency. Moen *et al.*[12] performed a study where blood was fractionated using DGM-based centrifugation, but the separated plasma and WBCs were not extracted into other chambers, rather the WBCs were trapped inside the BP chamber within a trough-like section. Then, an external microscope was used for imaging the trough-like sections resulting in 95% total WBC count. It showed that WBCs can be efficiently separated using the DGM-based centrifugation approach on a centrifugal microfluidic platform but indicates that while extracting the separated WBC/PBMC to another chamber, the efficiency decreases. However, the main purpose is to utilize the fractionated components for downstream biomedical applications, e.g., a metered plasma for biomarker detection as well as a separate chamber, which holds WBCs for cell counting and further processing. Thus, an efficient microfluidic approach is yet to be established for on-chip/disk extraction of the fractionated blood components into separate microfluidic chambers in an efficient manner.

Thus, in this study, we have adapted an event-triggered valving scheme;[29,30] in a hand-shake type of mode, the arrival of a liquid at a given position on the disk triggers the next step along the sample processing chain. Here, a small fraction of the separated plasma triggered the initial microfluidic event, i.e., the extraction of plasma from the BP chamber, which subsequently led to the extraction of PBMC into the cell counting chamber.[31,32] The plasma and the PBMCs were directed into distinct microfluidic chambers at a constant spin rate automated by event triggering, thus facilitating the potential integration of several sequential microfluidic steps for further processing of the fractionated component without changing the disk spin rate. Here, we use two different configurations of event-triggered valving: (i) basic event-triggered valving and (ii) event-triggered valving with "*overflow design*." The basic configuration demonstrates the core event-triggered valving mechanism where DGM-based centrifugation prompts the on-disk extraction of plasma and PBMC into separation; on the other hand, in the novel "overflow design" for density layer extraction, the fractionated plasma and PBMC are extracted by the overflow of liquid from the blood processing chamber to designated chambers. It was found that the overflow configuration of the event-triggered valving method eliminated the phase switching effect and consequently most of the PBMCs were flowed into the cell counting chamber. The cell counting was performed on-disk using an automated optical imaging unit (oCelloScope, BioSense Solutions ApS, Denmark), which is a combination of bright field and confocal microscopy facilitating capturing all the cells in focus.

II. EXPERIMENTAL

A. Materials and chemicals

Polymeric microfluidic disks fabricated in-house were used as the experimental platform in the study. EDTA-treated blood samples drawn from a healthy subject were purchased from Copenhagen University Hospital (Rigshospitalet, Denmark). 10 mM PBS (Sigma-Aldrich) was used for blood dilution. A DGM (Sigma-Aldrich, Histopaque-1077) adjusted to a density of 1077 g ml^{-1} was used for efficient separation between red blood cells (RBCs) and PBMCs. A commercial optical imaging unit with a customized disk-holder was used for on-disk PBMC scanning and counting.[14] Two different grades of polymeric dissolvable films (DF) mainly made of polyvinyl alcohol (PVA) that disintegrate in water or organic solvents, respectively, were used in this study: (i) embroidery film, which is a low-cost DF used for embroidery (Barnyarns, Ripon, UK; Avalon), and (ii) KC-35 film (Aciello Corporation, Japan). The dissolution time of the DFs depends on their chemical composition, e.g., embroidery film and KC-35 film dissolve within approximately 10 and 30 s, respectively, upon exposure to DI water. The DFs with different dissolution times were chosen in order to maintain the sequence and timing of the associated events. In addition to circular DFs, slot-shaped DFs were used prevent full submerging of the films prior to their dissolution; otherwise, it could create an airlock, which would impede the venting of the associated microchannel. The DF film is ∼35 μm thick and

so, depending on the DF shape, it has a dissolved volume of ~35–100 nl. This means each DF represents a dissolved volume of polyvinyl alcohol of less than 0.09% of the total assay volume. In a prior work, Gorkin *et al* validated the biocompatibility of these dissolvable films at these concentrations and found no measurable impact on bioassay performance.[33]

B. Microfluidic disk fabrication

In this study, the platform for all experiments was a poly (methyl methacrylate) (PMMA)-based microfluidic disk onto which the entire assay was integrated from sample pre-treatment to PBMC quantification. The disks were comprised of eight individual layers involving four layers of PMMA and four layers of pressure sensitive adhesive (PSA) with a multi-layered structure of microchannels [Fig. 1(a)].[34] The microchannels, being distributed in two different layers, facilitated crisscrossing of the microchannels as well as enabled the lower-layer microchannels to connect the chambers on the upper layer, thus increasing the design flexibility and the possibility to integrate more operational units on the disk. The disk-shaped substrate along with the microfluidic chambers as well as the vent and load holes were cut using a CO_2 laser on a PMMA sheet. The microchannels and microchambers were patterned on the PSA layers using a knife-cutter (Graphtec, Yokohama, Japan).

The PMMA and PSA layers were assembled in a bottom-up approach, and the disk layers were aligned using an alignment jig. The top PMMA layer with vent and load holes acted as the cover while the other PMMA layer represented the base. The lower microchannels defined in layer 7 were connected with certain chambers in layer 3 through the vertical vias accommodated in layer 6. The circular and slot-shaped DF tabs were fabricated[33] and attached as tabs onto the PSA layer. The "DF support" layer (layer 5) contained certain pockets for affixing these DF tabs, and the "DF cover" layer sandwiched the tabs in place. The upper microchannels defined in layer 2 were connected to certain chambers of layer 3. The eight-layered disk was bonded using a hot roll laminator (ChemInstruments, USA). Further details of the fabrication and assembling process can be found in previous studies.[29,30,34,35] The selection of dissolvable film valving was based on its high-reliability even when using relatively low-fidelity manufacturing techniques such as xurography.[34] Unlike conventional capillary valves, whose opening frequencies are highly reliant on interfacial tension and valve geometry,[36] DF valves actuation frequency is depending primarily on the volume of the valve. The geometry used in this work has been shown to support actuation frequency bands of ±1.8 Hz.[35] In this work, the DF burst valves are tuned to open in steps of 10 Hz (at 45 Hz in design 1 and at 35 and 45 Hz in design 2), which is within proven tolerance for this valve type. Furthermore, the event-triggered valves[29] used in both designs uses an actuation method based on "pneumatic hand-shaking." This technology is sufficiently reliable to enable 20+ sequential valving steps be implemented on a single disk.[30] During experiments associated with this manuscript, once the disk architectures were finalized, there were no valving related failures of our disks during experimentation.

C. Experimental procedure

1. Basic event-triggered valving

The whole microfluidic process to extract plasma and PBMCs from whole blood using event-triggered valving mechanism is illustrated in Fig. 2. The disk was first mounted on a "spin-stand" test instrument.[37,38] This is a spindle motor (Faulhaber, Minimotor, SA, Switzerland), which is controlled, via a CANOpen interface, using a custom LabVIEW program.[39] This motor has integrated functionality such that it can generate a 24-V step pulse as it passes a particular angular position (defined by the LabVIEW based UI). Custom electronics step this signal down to 5 V where it triggers image acquisition using a short exposure-time camera (Pixelfly, PCO, Germany) and a strobe light (Drelloscop 3244, Drello, Germany). This permits acquisition of a sequence of stationary frames, each at the same angular position during disk rotation, thus facilitating visualization of fluidic movement.

Then, 55 μl of DGM was loaded into the blood processing (BP) chamber by centrifugation of the disk at 25 Hz. Next, 13.75 μl of human whole blood was diluted in PBS with a volume ratio of 1:4 to facilitate better isolation of the PBMCs at the later stage of the experiment. The diluted blood (55 μl) was loaded into the disk using centrifugation speed of 35 Hz with a low acceleration (2.5 Hz/s) rate causing the blood to overlay over the DGM surface [Fig. 2(c-i)] followed by fractionation into plasma, PBMC band, and RBCs [Fig. 2(c-ii)].

At a spin rate of 35 Hz, the shock interface between the blood and supernatant plasma began approaching the pneumatic chamber [Fig. 2(c-ii)]; it stops at DF valve-1 while the centrifugal pressure is balanced by the pressure in the pneumatic chamber. This pneumatic pressure, according to Boyle's law can be expressed as

$$P = P_0 \frac{1}{1 - \Delta V/V}, \tag{1}$$

where P_0 is the ambient pressure, V is the volume of the pneumatic chamber that is initially occupied by air, and ΔV represents the reduction in the air volume due to the approaching blood/plasma meniscus.

The volume of the pneumatic chamber V was designed to burst the capillary valve-1 at approximately 45 Hz. Thus, after blood fractionation, the centrifugal speed was increased to 45 Hz to overcome the pneumatic pressure (P), which subsequently caused the bursting of DF valve-1 and led some amount of plasma to get in contact with DF1 [Fig. 2(c-iii)]. As the DF1 dissolved after being wetted by plasma for about 10 s, the lower channel-1 was vented, and the blood plasma was able to flow through this lower microchannel to the plasma-holding (PH) chamber [Fig. 2(c-iv)]. Afterward, approximately 8 μl of plasma entered the plasma chamber through a connecting microchannel, which can be used for further processing, e.g., for biomarker detection. In the meantime, the slot-shaped DF2 being wetted with plasma eventually dissolved, which vented pneumatic channel-2. Subsequent to opening DF valve-2, some DGM contacted and thus dissolved DF3 to vent the lower channel-3 so that the remaining plasma, PBMCs, and some amount of DGM entered the cell counting (CC) chamber [Fig. 2(c-v)]. However, it was observed that there was some dead volume in capillary valve-2, which likely contained some PBMCs

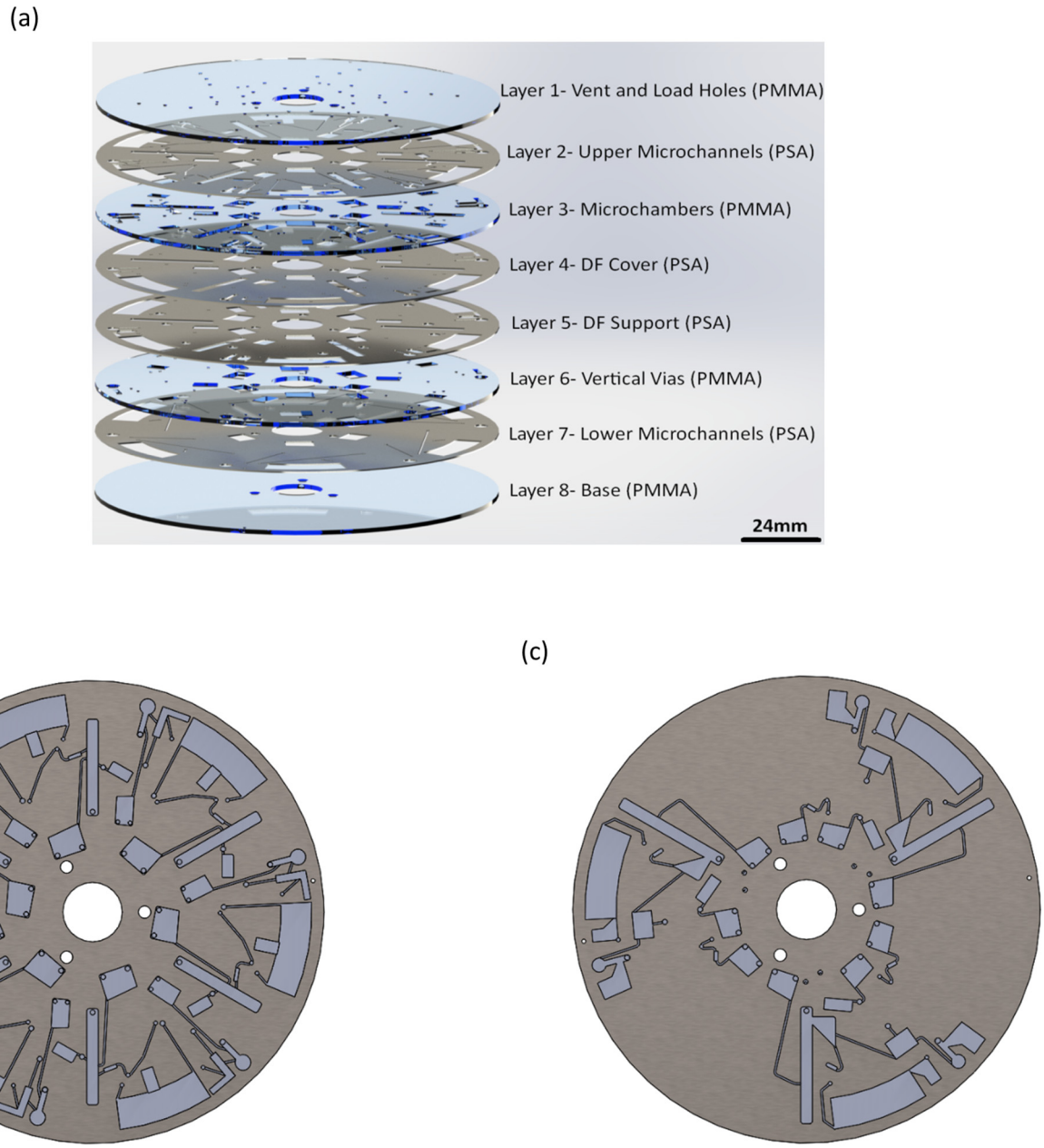

FIG. 1. (a) Schematics of the assembly of the multi-layer disks with dissolvable valves and multi-layered microchannels. (b) Schematics of the top-down view of the basic event-triggered design. (c) Schematics of top-down view of the "overflow" design.

[Fig. 2(c-vi)]. The CC chamber was finally scanned using an integrated optical imaging unit to perform on-disk PBMC counting.

2. Event-triggered valving with "overflow design"

In the second microfluidic design (hereafter named "overflow design"), the plasma and the PBMCs were sequentially overflowed (rather than extraction) into two different chambers using additional DGM through multi-layered microchannels. Here, the sequence of events was controlled by four DFs positioned at specific locations of the disk (Fig. 3).

In this design, 60, 55, and 20 μl DGM were pre-loaded, respectively, in the blood processing (BP) chamber, "overflowing DGM-1" (OD-1) chamber, and "overflowing DGM-2" (OD-2) chamber.

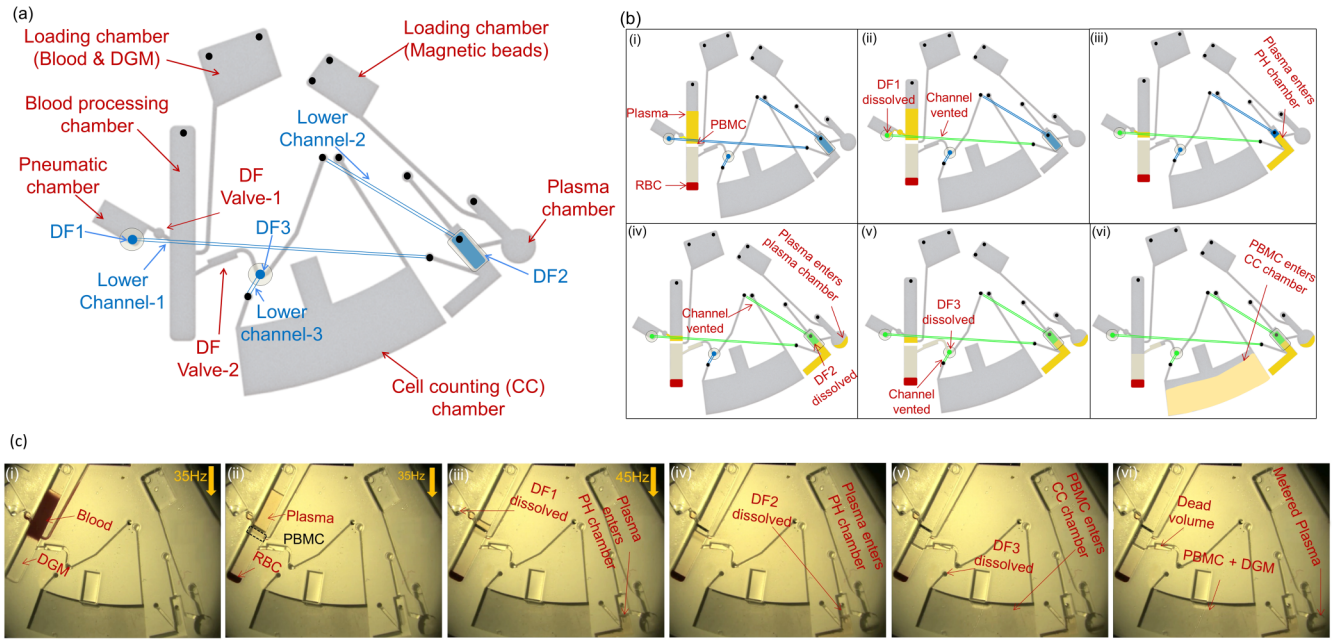

FIG. 2. (a) Schematic of a single functional unit of the microfluidic disk with the basic event-triggered valving design. (b) Sequence of the entire microfluidic process. The lower channels are marked with blue when pressurized and marked with green when vented. Similarly, the DF valves are marked with blue when intact and marked with green when dissolved. The three DFs are numbered (e.g., DF1, DF2) according to the sequence of their dissolution. (c) Picture frames of the event-triggered mechanism to sequentially forward plasma and PBMCs to their distinct receiving chambers.

OD-1 and OD-2 chambers were connected to the BP chamber through lower microchannels [Fig. 3(b)]. The purpose of the additional DGM was that the DGM in OD-1 chamber would enter the BP chamber to overflow the fractionated plasma into the overflow chamber and later into the plasma chamber; and the DGM in OD-2 chamber would similarly enter the BP chamber to overflow the PBMC layer along with some DGM into the CC chamber.

After loading the DGM in the designated chambers, 60 μl of PBS-diluted blood (blood: PBS = 1:4) was added to the BP chamber using a centrifugation speed of 30 Hz with a low acceleration (2.5 Hz s^{-1}) rate resulting in the blood to fractionate into plasma, PBMCs, and RBCs likewise the earlier design [Fig. 3(c-i)]. Then, the spin rate was increased to 35 Hz resulting in bursting of the capillary valve-1, which eventually led the DGM in OD-1 to wet DF1 [Fig. 3(c-ii)]. After the DF1 was dissolved and wetted by DGM for about 30 s, the DGM entered the BP chamber through the lower channel, which overflowed the plasma to the overflow chamber [Fig. 3(c-ii)]. Through the connecting microchannels, the overflowed plasma entered the plasma chamber via PH chamber [Figs. 3(c-iii) and 3(c-iv)]. Upon contact with plasma in the PH chamber, the DF2 was wetted and eventually dissolved to vent the associated lower microchannel [Fig. 3(c-iii)]. This way, the air pressure to get reduced in the associated lower microchannel and, thus, the remaining overflowed plasma was able to approach further and eventually contacted DF3 through the associated lower microchannel. Subsequently, the dissolution of DF3 led the overflowed plasma to enter the CC chamber via the connecting microchannel [Fig. 3(c-iv)]. Next, the disk spin rate was increased to 45 Hz, which caused the DGM in OD-2 to burst the DF valve-2 and wet DF4 [Fig. 3(c-v)]. Being wetted with DGM for about 30 s, the DF4 was dissolved, which led the DGM to enter the BP chamber through the associated lower microchannel and eventually overflowed the PBMC band along with some DGM first into the overflow chamber and then to CC chamber [Fig. 3(c-vi)]. The microchannel associated with the CC chamber that is connected at the very bottom of the chamber and due to constant centrifugation, the PBMCs, and other cells were ensured to be distributed at the bottom of the chamber and the excess plasma to be in the waste chamber. The entire microfluidic process is captured in the video in the supplementary material.

III. RESULTS AND DISCUSSION

The PBMCs were quantified on-disk using the automated optical imaging unit (demonstrated in S2 in the supplementary material). As the PBMCs were held in the CC chamber with a thickness of 86 μm, the cells were expected to be randomly distributed in a monolayer. Such distribution assisted the imaging unit to capture all the cells in focus.

An object-based image analysis algorithm embedded in the instrument software Uniexplorer was used for the segmentation and quantification of the PBMCs. Plasma mixed with the PBMCs in the CC chamber; platelets and a few RBCs were observed in the raw scanned images along with the PBMCs [Fig. 4(a)]. The

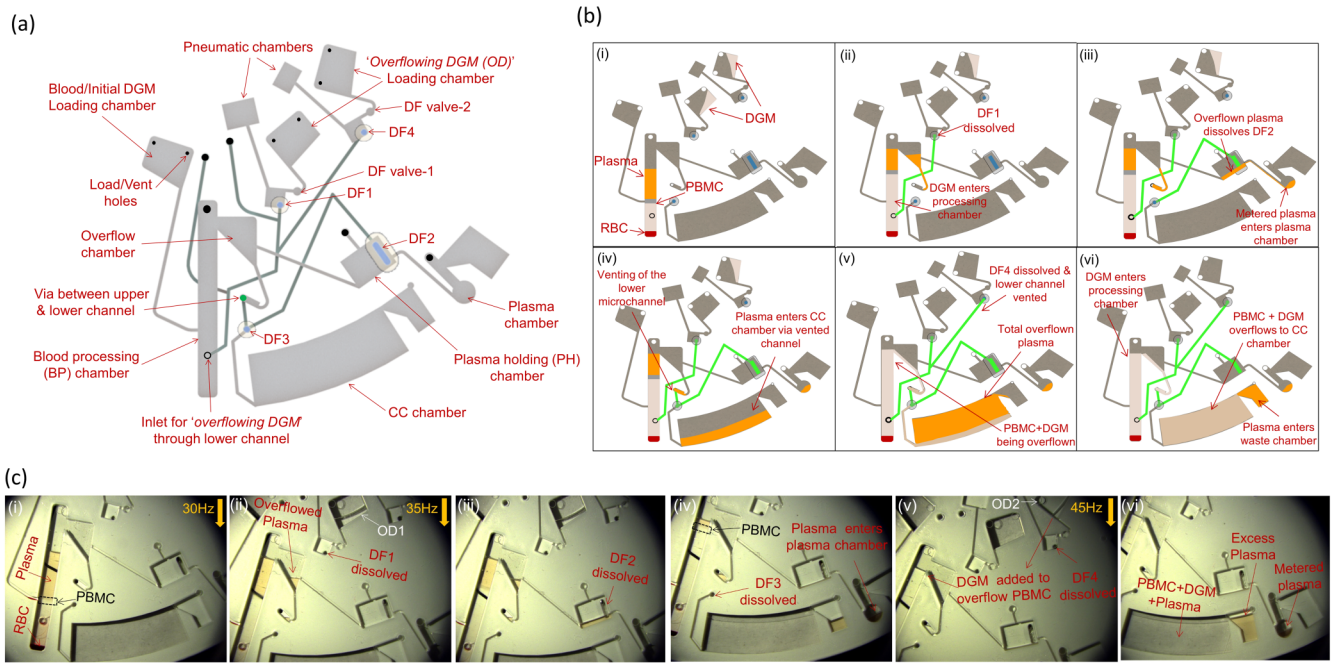

FIG. 3. (a) Schematic of the overflow design as an operational unit of the microfluidic disk. The four DFs (blue-colored) are numerically named (e.g., DF1, DF2) indicating the sequence of their dissolution. The microchannels are embedded into two separate layers so that the microchannels at the lower layer (bottle green-colored) can pass beneath the chambers on the upper layer. (b) Representative schematics of the entire microfluidic process. The lower channels are marked with blue when pressurized and marked with green when vented. Similarly, the DF valves are marked with blue when intact and marked with green when dissolved. The four DFs are numbered (e.g., DF1, DF2) according to the sequence of their dissolution. (c) Frame sequence of plasma and PBMC separation using the overflow design. (i) Blood is fractionated into plasma, PBMC, and RBC by DGM-based centrifugation. (ii) Elevation of the spin rate drives DGM in OD1 to dissolve DF1. The dissolution of DF1 enables DGM in OD1 to enter the BP chamber through lower microchannel to increase the liquid column height and eventually leading to plasma overflow into the outlet. (iii) The overflowed plasma enters the PH chamber and dissolves DF2. (iv) The plasma enters the plasma chamber from the PH chamber and the dissolution of DF2 triggers the venting of associated pneumatic lower microchannel causing DF3 to be dissolved by the remaining plasma in overflow chamber. The dissolution of DF3 enables the remaining plasma to enter the CC chamber. (v) Further elevation of the spin rate leads DGM in OD2 to dissolve DF4 and enter the BP chamber through lower microchannel causing the overflow of PBMC to the overflow chamber and subsequently to the CC chamber. (vi) PBMCs along with some plasma and DGM are held in the CC chamber for quantification by optical imaging.

segmentation algorithm distinguishes the cells based on their surface area and, thus, the platelets being significantly smaller (2 μm) than the PBMCs (7–30 μm) were eliminated after the segmentation process [Fig. 4(b)]. However, smaller RBCs. which are of the same size range as small lymphocytes (7–8 μm), remained alongside the PBMCs after the segmentation [Fig. 4(b)]. Nevertheless, by virtue of their biconcave shape, these RBCs were manually identified and eliminated from the segmented images and, thus, finally only the PBMCs were quantified by counting the number of segmented images by the software [Fig. 4(c)].

Figure 4(d) demonstrates the PBMC count/μl of a sample collected from a healthy subject and compares the PBMC extraction efficiency between the two valving strategies against a standard cell counting method, i.e., flow cytometry (Sysmex Europe GmbH) performed in Copenhagen University hospital. Comparing with the standard clinical measurement, it shows that using the basic event-triggered method, approximately 64% of total PBMCs were extracted, whereas using the overflow design, the extraction efficiency was increased to about 88%.

In the basic event-triggered valving strategy, the dead volume containing PBMCs inside capillary valve-2 along with the observed phase switching effect (shown Sec. S1 in the supplementary material) are the potential reasons for the lower PBMC extraction efficiency. Here, the pressure created by the centrifugal force led the PBMCs to flow into the CC chamber while some PBMCs remained back in the BP chamber, whereas in our previous study,[1] it was the pneumatic pressure that caused the PBMCs to be extracted from the BP chamber. Thus, it shows that extraction of PBMCs by centrifugal or pneumatic pressure would not be a preferred option for increasing the extraction efficiency. On the contrary, in the overflow design, the additional DGM being denser than the PBMC band acted as the carrier of the cells down to the CC chamber. No remaining PBMC band was observed in this design as shown Sec. S1 in the supplementary material. This illustrates that the DGM carried all the PBMCs effectively into the CC chamber for which we obtained 88% extraction efficiency. The remaining 12% of PBMCs might have been lost in the BP chamber during fractionation as the Histopaque-1077 cannot separate 100% PBMCs.[40]

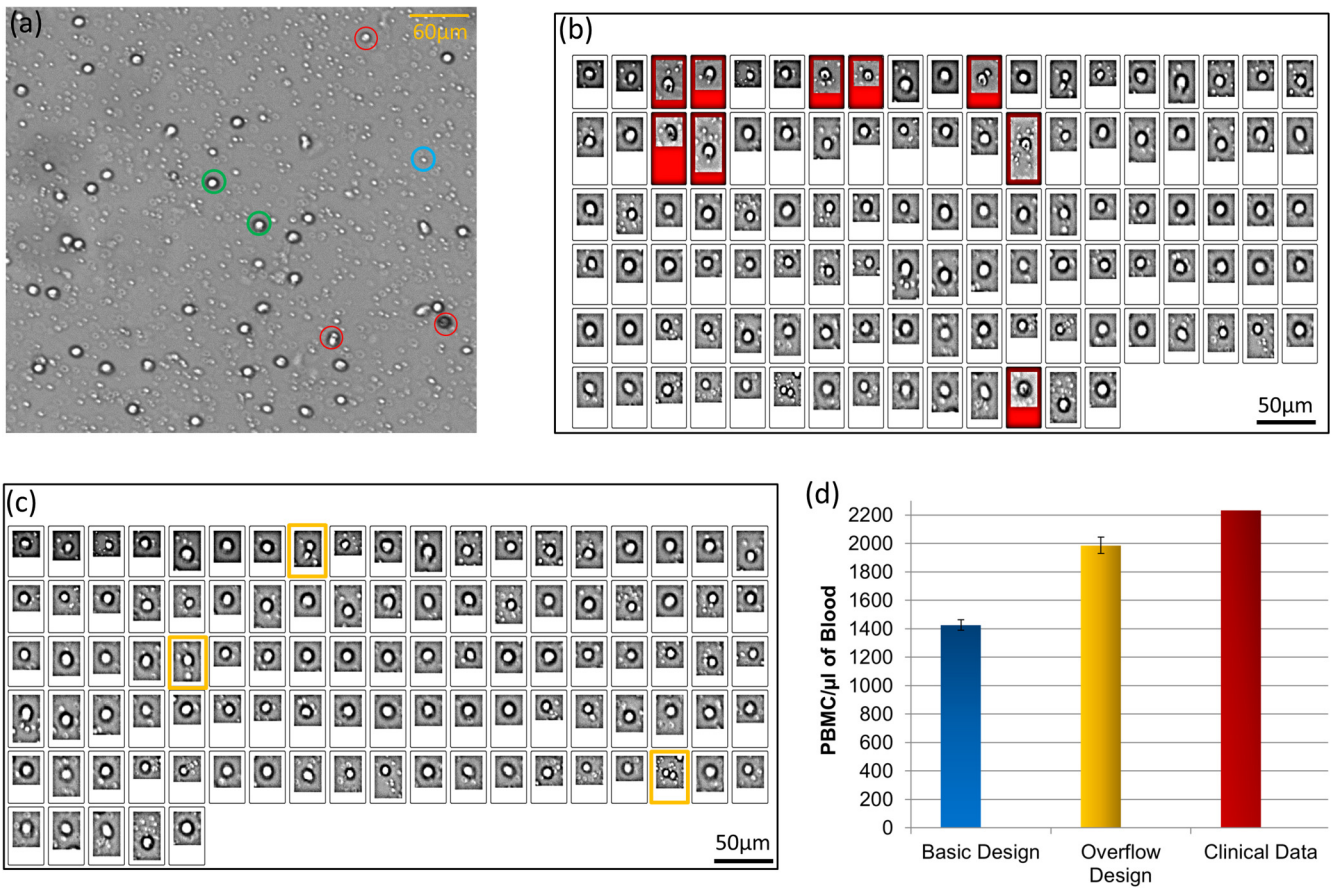

FIG. 4. (a) A raw image of a part of the CC chamber scanned by the imaging unit. Platelets (blue-circled) and RBCs (red-circled) can be seen in the pool of PBMCs (green-circled). Only two PBMCs have been marked with green for presentation purpose. (b) A view of the segmented images after the segmentation process demonstrating some RBC contamination (red-marked). (c) A view of the segmented images containing only PBMCs after the deletion of the segmented RBCs. The orange-marked segmented images shows that there are few cases where two adjacent cells are counted as one segmented image, which reduces the count of PBMCs present in the CC chamber. (d) PBMC quantification data from one healthy subject comparing the PBMC count among the basic design, overflow design, and the clinical data. The error bars represent the standard deviation obtained from triplicate measurements.

Another potential reason is the limitation of the counting algorithm; as in some cases, where two PBMCs were very adjacent or sticked to each other, these were counted as one segmented object, which have reduced the number of PBMC count.

IV. CONCLUSION

We have presented a new centrifugal microfluidic strategy to efficiently extract metered plasma and PBMCs from a single blood sample into separate microfluidic chambers for downstream biomedical applications. The plasma volume can be used as a sample for detecting biomarkers, e.g., by adding functionalized magnetic beads to detect specific analytes. The demonstration of the on-disk PBMC counting by an imaging unit and a segmentation algorithm eliminates the need for PBMC purification from contaminants. The utilization of the event-triggered valving with multi-layered microchannels increased automation of the process through the usage of DF valves; and further, it holds potential for the convenient addition of similar DF-based units to multiplex further processing steps, e.g., separating monocytes and lymphocytes from the extracted PBMCs.

The overflow design strategy utilized DGM as the vehicle for transporting both plasma and PBMCs separately to different chambers while being independent of any pneumatic or centrifugal pressure. This particular extraction strategy can potentially be utilized for effectively separating different density layers from a liquid column for several biomedical applications, e.g., nanoparticle purification, cell sorting, or DNA isolation. This strategy eliminated the probability of the phase switching effect during extracting PBMCs, which resulted in a significant increase in the extraction efficiency. Previously, Kinahan *et al.*[13] reported an extraction efficiency of 34% using side-mounted outlet channels and identified "phase switching" as the cause of this low performance. Our "overflow" based method of removing the white blood cells significantly improves the extraction efficiency to 88% and, therefore, matches

or even out-performs benchtop density-gradient based isolation methods.

This integrated approach to extracting PBMCs with high efficiency also has potential to provide an automated sample preparation step for other assays. In this case, rather than analyzing PBMCs on the disk, they might be removed for separate analysis or to be placed into long-term storage. In conventional disks, PBMCs might be removed through a (normally sealed) vent at the base of the sample collection chamber.[13] The ability to integrate a collection tube directly into a centrifugal analysis platform has also been demonstrated[41,42] and can offer the potential for low-loss and closed-tube transfer of samples to downstream assays, compatible lab-instruments, or into long-term storage.

In the future, to specifically quantify the PBMC extraction efficiency of the overflow structure, more clinical samples need to be tested. Furthermore, in order to quantify the accuracy of the on-disk counting algorithm, the separated PBMCs need to be extracted from the disk and counted with a standard hemocytometer followed by a comparison with the on-disk count.

SUPPLEMENTARY MATERIAL

See the supplementary material for the experimental details of the microfluidic operation as well as the optical imaging details.

ACKNOWLEDGMENTS

The research leading to these results has received funding from the European Research Council under the European Union's Seventh Framework Programme (No. FP7/2007-2013)/ERC under (Grant Agreement No. 320535), from the Center of Excellence "IDUN" granted by the Danish National Research Foundation (Grant No. DNRF122), and from the Velux Foundations.

AUTHOR DECLARATIONS

Conflict of Interest

The authors have no conflicts to disclose.

DATA AVAILABILITY

The data that support the findings of this study are available from the corresponding author upon reasonable request.

REFERENCES

[1]R. Uddin, M. Donolato, E.-T. Hwu, M. F. Hansen, and A. Boisen, Sens. Actuators B **272**, 634 (2018).
[2]M. Madou, J. Zoval, G. Jia, H. Kido, J. Kim, and N. Kim, Annu. Rev. Biomed. Eng. **8**, 601 (2006).
[3]J. Ducrée, S. Haeberle, S. Lutz, S. Pausch, F. Von Stetten, and R. Zengerle, J. Micromech. Microeng. **17**, S103 (2007).
[4]R. Gorkin, J. Park, J. Siegrist, M. Amasia, B. S. Lee, J.-M. Park, J. Kim, H. Kim, M. Madou, and Y.-K. Cho, Lab Chip **10**, 1758 (2010).
[5]S. Smith, D. Mager, A. Perebikovsky, E. Shamloo, D. Kinahan, R. Mishra, S. Torres Delgado, H. Kido, S. Saha, and J. Ducrée, Micromachines **7**, 22 (2016).
[6]M. Amasia and M. Madou, Bioanalysis **2**, 1701 (2010).
[7]W. S. Mielczarek, E. A. Obaje, T. T. Bachmann, and M. Kersaudy-Kerhoas, Lab Chip **16**, 3441 (2016).
[8]J. N. Kuo and X. F. Chen, Microsyst. Technol. **21**, 2485 (2015).
[9]U. Y. Schaff, A. M. Tentori, and G. J. Sommer, "Differential white cell count by centrifugal microfluidics," in the *14th International Conference on Miniaturized Systems for Chemistry and Life Sciences, Groningen, The Netherlands, 3–7 October 2010* (CBMS, 2010).
[10]D. J. Kinahan, S. M. Kearney, M. T. Glynn, and J. Ducrée, Sens. Actuators A **215**, 71 (2014).
[11]M. Rombach, S. Zehnle, N. Paust, M. Weil, Ö Sogukpinar, R. Zengerle, and M. Karle (n.d.), "Microfluidic App for Buffy Coat Extraction From Large Peripheral Blood Samples for Low-Abundance Living-Cell Analysis," in *International Conference on Miniaturized Systems for Chemistry and Life SciencesAt: 25–29 October 2015 Gyeongju, Korea* (CBMS, 2015) Vol. 19, pp, 1172–1174.
[12]S. T. Moen, C. L. Hatcher, and A. K. Singh, PLoS ONE **11**, e0153137 (2016).
[13]D. J. Kinahan, S. M. Kearney, N. A. Kilcawley, P. L. Early, M. T. Glynn, and J. Ducrée, PLoS ONE **11**, e0155545 (2016).
[14]R. Uddin, R. Burger, M. Donolato, J. Fock, M. Creagh, M. F. Hansen, and A. Boisen, Biosens. Bioelectron. **85**, 351 (2016).
[15]H. Y. Tsai, C. F. Hsu, I. W. Chiu, and C. Bor Fuh, Anal. Chem. **79**, 8416 (2007).
[16]C. S. Thaxton, C. A. Mirkin, and J. Nam, Science **301**(80), 1884 (2003).
[17]H. Park, M. P. Hwang, and K. H. Lee, Int. J. Nanomed. **8**, 4543 (2013).
[18]H. E. Horng, S. Y. Yang, C. Y. Hong, C. M. Liu, P. S. Tsai, H. C. Yang, and C. C. Wu, Appl. Phys. Lett. **88**, 252506 (2006).
[19]J. K. Herr, J. E. Smith, C. D. Medley, D. Shangguan, and W. Tan, Anal. Chem. **78**, 2918 (2006).
[20]A. Hecht, P. Commiskey, N. Shah, and R. Kopelman, Biosens. Bioelectron. **48**, 26 (2013).
[21]M. Donolato, P. Antunes, T. Z. G. de la Torre, E. Te Hwu, C. H. Chen, R. Burger, G. Rizzi, F. G. Bosco, M. Strømme, A. Boisen, and M. F. Hansen, Biosens. Bioelectron. **67**, 649 (2015).
[22]M. Donolato, P. Antunes, R. S. Bejhed, T. Zardán Gómez De La Torre, F. W. Østerberg, M. Strömberg, M. Nilsson, M. Strømme, P. Svedlindh, M. F. Hansen, and P. Vavassori, Anal. Chem. **87**, 1622 (2015).
[23]S. Centi, G. Messina, S. Tombelli, I. Palchetti, and M. Mascini, Biosens. Bioelectron. **23**, 1602 (2008).
[24]R. S. Bejhed, T. Zardán Gómez de la Torre, P. Svedlindh, and M. Strömberg, Biotechnol. J. **10**, 469 (2015).
[25]R. S. Bejhed, T. Zardán Gómez De La Torre, M. Donolato, M. F. Hansen, P. Svedlindh, and M. Strömberg, Biosens. Bioelectron. **66**, 405 (2015).
[26]J. Fock, C. Jonasson, C. Johansson, and M. F. Hansen, Phys. Chem. Chem. Phys. **19**, 8802 (2017).
[27]R. Uddin, N. E. Habiba, G. Rena, E. Te Hwu, and A. Boisen, ACS Sens. **2**, 7b00384 (2017).
[28]M. Fredborg, K. R. Andersen, E. Jørgensen, A. Droce, T. Olesen, B. B. Jensen, F. S. Rosenvinge, and T. E. Sondergaard, J. Clin. Microbiol. **51**, 2047 (2013).
[29]D. J. Kinahan, S. M. Kearney, N. Dimov, T. Glynn, and J. Ducrée, Lab Chip **14**, 2249 (2014).
[30]D. J. Kinahan, S. M. Kearney, O. P. Faneuil, M. T. Glynn, N. Dimov, and J. Ducrée, RSC Adv. **5**, 1818 (2015).
[31]A. Kazarine, M. C. R. Kong, E. J. Templeton, and E. D. Salin, Anal. Chem. **84**, 6939 (2012).
[32]S. M. Torres Delgado, D. J. Kinahan, L. A. Nirupa Julius, A. Mallette, D. S. Ardila, R. Mishra, C. M. Miyazaki, J. G. Korvink, J. Ducrée, and D. Mager, Biosens. Bioelectron. **109**, 214 (2018).
[33]R. Gorkin III, C. E. Nwankire, J. Gaughran, X. Zhang, G. G. Donohoe, M. Rook, R. O'Kennedy, and J. Ducrée, Lab Chip **12**, 2894 (2012).
[34]D. J. Kinahan, P. L. Early, A. Vembadi, E. MacNamara, N. A. Kilcawley, T. Glennon, D. Diamond, D. Brabazon, and J. Ducrée, Lab Chip **16**, 3454 (2016).
[35]R. Mishra, J. Zapatero-Rodríguez, S. Sharma, D. Kelly, D. McAuley, S. Gilgunn, R. O'Kennedy, and J. Ducrée, Sens. Actuators B **263**, 668 (2018).
[36]H. Cho, H.-Y. Kim, J. Y. Kang, and T. S. Kim, J. Colloid Interface Sci. **306**, 379 (2007).

[37]M. Grumann, T. Brenner, C. Beer, R. Zengerle, and J. Ducrée, Rev. Sci. Instrum. **76**, 25101 (2005).
[38]D. Brennan, H. Coughlan, E. Clancy, N. Dimov, T. Barry, D. Kinahan, J. Ducrée, T. J. Smith, and P. Galvin, Sens. Actuators B **239**, 235 (2017).
[39]S. M. T. Delgado, D. J. Kinahan, F. S. Sandoval, L. A. N. Julius, N. A. Kilcawley, J. Ducrée, and D. Mager, Lab Chip **16**, 4002 (2016).
[40]H. W. Grievink, T. Luisman, C. Kluft, M. Moerland, and K. E. Malone, Biopreserv. Biobanking **14**, 410 (2016).
[41]D. Brassard, M. Geissler, M. Descarreaux, D. Tremblay, J. Daoud, L. Clime, M. Mounier, D. Charlebois, and T. Veres, Lab Chip **19**, 1941 (2019).
[42]A. Kazemzadeh, A. Eriksson, M. Madou, and A. Russom, Nat. Commun. **10**, 189 (2019).